tvst

Article

Corneal Biomechanics After Intrastromal Ring Surgery: Optomechanical In Silico Assessment

Miguel Ángel Ariza-Gracia[1,#], Julio Flecha-Lescún[2,#], Philippe Büchler[1], and Begoña Calvo[2,3]

[1] ARTORG Center for Biomedical Engineering Research, Faculty of Medicine, University of Bern, Bern, Switzerland
[2] Aragón Institute for Engineering Research (i3A), University of Zaragoza, Zaragoza, Spain
[3] CIBER in Bioengineering, Biomaterials & Nanomedicine (CIBER-BBN), Madrid, Spain

Correspondence: Miguel Ángel Ariza-Gracia, ARTORG, Faculty of Medicine, University of Bern, Bern, Switzerland. e-mail: miguel.ariza@artorg.unibe.ch

Received: June 4, 2020
Accepted: September 10, 2020
Published: October 21, 2020

Keywords: intrastromal implants; in silico models; corneal biomechanics; high myopia; keratoconus

Citation: Ariza-Gracia MÁ, Flecha-Lescún J, Büchler P, Calvo B. Corneal biomechanics after intrastromal ring surgery: Optomechanical in silico assessment. Trans Vis Sci Tech. 2020;9(11):26, https://doi.org/10.1167/tvst.9.11.26

Purpose: To provide a biomechanical framework to better understand the postsurgical optomechanical behavior of the cornea after ring implantation.

Methods: Calibrated in silico models were used to determine the corneal shape and stresses after ring implantation. After mechanical simulations, geometric ray-tracing was used to determine the change in spherical equivalent. The effect of the surgical procedure, circadian variation of intraocular pressure, or the biomechanical weakening introduced by keratoconus (KC) were evaluated for each intrastromal ring.

Results: Models predicted the postsurgical optomechanical response of the cornea at a population level. The localized mechanical effect of the additional intrastromal volume introduced by the implants (size and diameter) drives the postsurgical corneal response. However, central corneal stresses did not increase more than 50%, and thus implants did not strengthen the cornea globally. Because of the biomechanical weakening introduced by laser pocketing, continuous implants in a pocket resulted in higher refractive corrections and in the relaxation of the anterior stroma, which could slow down KC progression. Implants can move within the stroma, acting as a dynamic pivot point that modifies corneal kinematics and flattens the corneal center. Changes in stromal mechanical properties did not impact on refraction for normal or pathological corneas.

Conclusions: Implants do not stiffen the cornea but create a local bulkening effect that regularizes the corneal shape by modifying corneal kinematics without canceling corneal motion.

Translational Relevance: In silico models can help to understand corneal biomechanics, to plan patient-specific interventions, or to create biomechanically driven nomograms.

Introduction

Intrastromal ring segments (IRS or ICRS) or intrastromal continuous rings (ICR) are small polymeric devices that are introduced in the corneal stroma to regularize the corneal surface and correct high refractive errors. This technique was originally introduced to treat patients suffering from keratoconus (KC),[1] but it was extended to other indications, such as marginal pellucid degenerations,[2] post-LASIK ectasia,[3] and high myopia, in which laser refractive correction is not possible.[4] Three main types of rings are now on the market: continuous rings (e.g., MyoRing, Dioptex GmbH), almost continuous ring segments covering an arc with a central angle between 320° and 355° (e.g., Keraring, Mediphacos, Belo Horizonte, Brazil), and IRS that cover angles below 210° and can be placed by pairs depending on the classification of the cone and amount of correction (e.g., Ferrara, Ophthalmic Ltd.; or Intacs, Addition Technology Inc.). Beside their difference in angular coverage, the existing systems differ by the design of their cross-section and diameter. Nomograms based on morphological parameters, such as the central corneal curvature, minimum corneal thickness,[5,6] or the KC

classification,[7] are used to plan the intervention and select the appropriate implant.

Surgical outcomes are characterized by a high variability,[8] thus controlling the postoperative biomechanics is a challenging issue, although several authors[4,5,9,10] reported that the smaller refractive correction owing to the larger diameter is not in contrast with the other observed effects. For example, the shape and size of the cross-section of the implant, its diameter and arc length (in the case of IRS), as well as its implantation position affect the postsurgical shape of the cornea and the respective refractive correction. Also, mechanical factors, such as intraocular pressure (IOP) and tissue biomechanics, play a role and should be accounted for when designing a nomogram.[4,5,7]

The implantation depth is one of the surgical parameters that was evaluated clinically. The recommended implantation depth is 75% to 80% of the stromal thickness. Hashemi et al.[11] stressed that for IRS there was an optimal range of stromal depth between 60% and 79% for which the refractive correction was maximal, whereas any other implantation depth had a low impact on the topographic outcomes. Barbara et al.[12] pointed out that the actual insertion depth observed in patients treated with IRS was shallower (∼60%) than the intended insertion depth (∼80%). This observation could be partly explained by the local variation of corneal thickness, whereas the surgical incision remains at a constant distance from the anterior surface but highlighted the difficulty of comparing and interpret existing clinical data. This 20% mismatch in implantation depth or the uncontrolled postsurgical rotation of the implant within the stroma[13] could impact the refractive outcomes.

Unlike the placement of ring segments inside an intrastromal tunnel, continuous rings require a complete intrastromal pocket,[14–16] which has important consequences on the mechanical stability after treatment as the pocket cuts a large surface of the cornea that can include both normal and pathological tissues.[17] Despite providing a higher refractive correction than ring segments, the mechanical impact of the intrastromal pocket remains unclear as it cannot be quantified in clinics. To estimate the mechanical impact of this treatment, Daxer[18] used the Laplace equation to calculate the strengthening corneal factor (SFC), a mechanical marker based on the ratio between the Cauchy stress (σ) in the corneal tissue before and after the ring implantation ($SFC = \sigma_{Before} / \sigma_{After}$). Using this simple approach, he estimated an SFC of 2 to 3 for continuous rings and an SFC of ∼1 for ring segments. In his opinion, this difference was explained by the fact that continuous rings restricted the corneal movement acting as an auxiliary limbus, which was not the case for ring segments. Based on this calculation, Daxer suggested that continuous rings were able to introduce a corneal strengthening that should avoid the progression of KC, whereas ring segments would not, as other clinical studies pointed out.[19–21] Nevertheless, other authors outlined the need for additional evidence to confirm this claim.[22]

Clinical studies showed that these implants regularized the corneal surface and provided a noticeable correction even for high myopia (>6 diopters [D]). However, planning the surgery to achieve a specific refractive outcome remains challenging.[10] The mechanical principle underlying this treatment remains poorly understood and is difficult to extract only from clinical studies.[8] As clinical studies often present mixed populations with different degrees of myopia, KC severity, or implant typology, it is not possible to isolate the contribution of each parameter on the refractive outcomes. In addition, mechanical properties of the cornea play an important role in the procedure but, unfortunately, it is not possible to characterize corneal biomechanics in vivo with current clinical devices. In silico models have been proposed to study the insertion of intrastromal rings,[9,23–26] however, to the best of our knowledge, no study systematically reported the individual contribution of the implant geometry, the surgical and mechanical parameters on the postsurgical refractive outcomes.

In the present study, we use a calibrated in silico model to understand the mechanical response of the cornea to the treatment and to estimate how different geometric and biomechanical parameters affect the refractive outcomes. Our hypothesis is that implants do not induce a corneal strengthening (change in stresses) but a local mechanical effect, which is a combination of the added volume and the position of the implant with respect to the corneal center, which modifies corneal kinematics and regularizes the corneal surface without introducing a great change in the central stromal stresses. More peripheral implants should have a lower impact on refraction as the localized mechanical effect will dissipate before reaching the corneal center.

Methods

In Silico Model of Intrastromal Corneal Rings Surgery

A normal cornea was modeled as a spherical dome with a symmetry of revolution around the optical axis (Y-axis, Fig. 1a.1). This geometric description is sufficient to capture the average curvature at the corneal

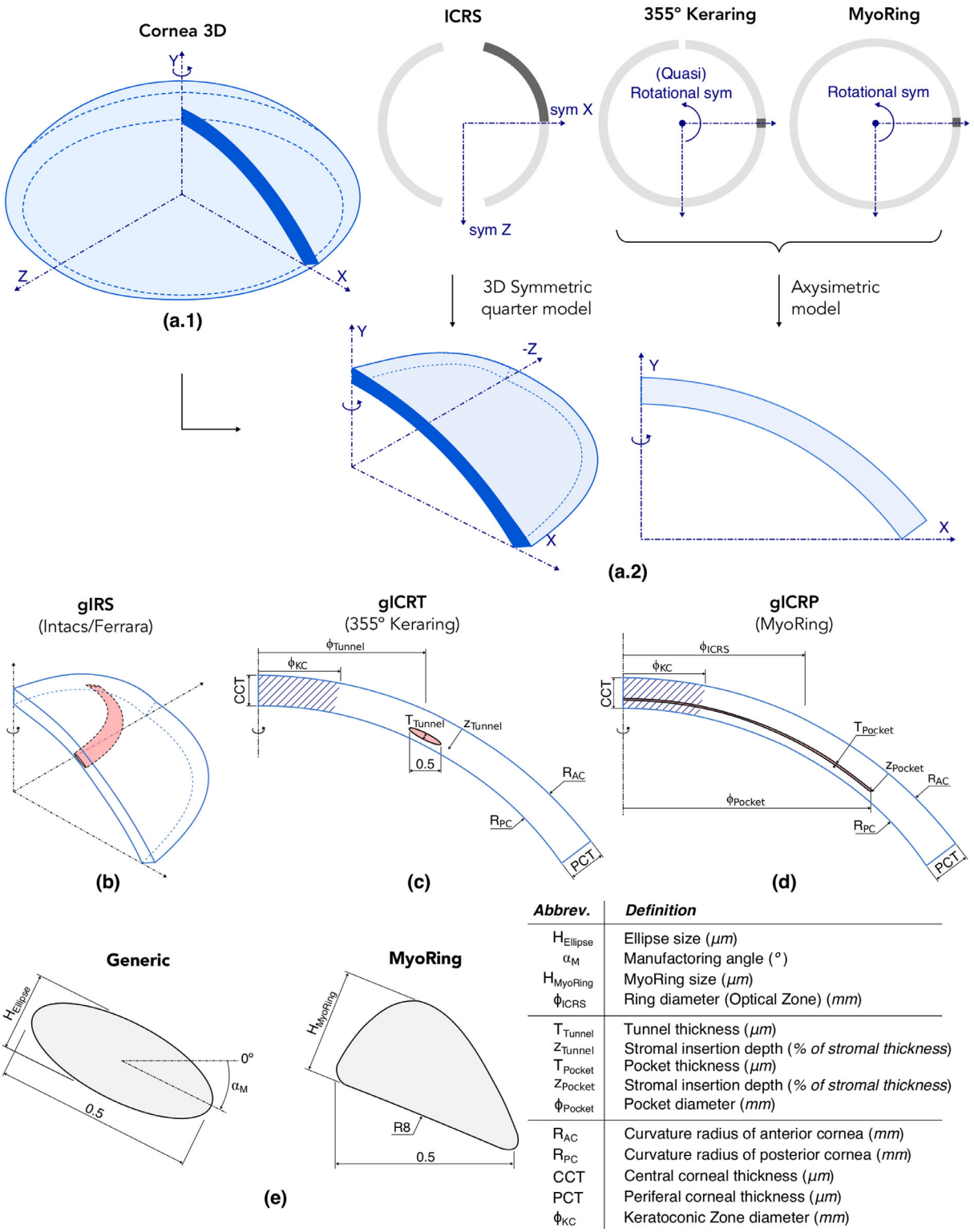

Abbrev.	*Definition*
$H_{Ellipse}$	Ellipse size (μm)
α_M	Manufactoring angle (°)
$H_{MyoRing}$	MyoRing size (μm)
ϕ_{ICRS}	Ring diameter (Optical Zone) (mm)
T_{Tunnel}	Tunnel thickness (μm)
z_{Tunnel}	Stromal insertion depth (% *of stromal thickness*)
T_{Pocket}	Pocket thickness (μm)
z_{Pocket}	Stromal insertion depth (% *of stromal thickness*)
ϕ_{Pocket}	Pocket diameter (mm)
R_{AC}	Curvature radius of anterior cornea (mm)
R_{PC}	Curvature radius of posterior cornea (mm)
CCT	Central corneal thickness (μm)
PCT	Periferal corneal thickness (μm)
ϕ_{KC}	Keratoconic Zone diameter (mm)

Figure 1. Schematic representation of the in silico models used in this study. (**a**) Symmetry of the model for different ring typologies. Y-axis is the axis of revolution (optical axis); (**b, c**) in silico models for implants in pocket: segments (gIRS) and continuous (gICRT); (**d**) in silico model for implants in pocket (MyoRing and gICRP); (**e**) implant's cross-section: generic and MyoRing.

Table 1. Presurgical Morphological Description of the In Silico Models

Case	Cone Radius [mm]	CCT [µm]	K_{mean} [D]	AL [mm]	SPS [mm]	SE [D]
High myopia	–	550	45	26.5	4	−9.4
$KC_{0.5}$	0.5	436	50	26.5	4	−11.1
KC_1	1.0	503	50	26.5	4	−11.9
$KC_{1.5}$	1.5	528	50	26.5	4	−11.5

CCT, central corneal thickness; K_{mean}, average central keratometry; AL, axial length; SPS, scotopic pupil size; SE, spherical equivalent.

center (K_{mean}) and the overall defocus of the optical system (Zernike coefficient, Z_2^0 and spherical equivalent [SE]). For the sake of simplicity, only corneas with central KC were considered to preserve the symmetry of revolution even if they are exceptional cases in clinics. Four different corneal topologies were considered in this study: one cornea with high myopia and three pathological corneas with a central KC of different severity. The mechanical properties of the cornea corresponded to those of a normal tissue except in the region of the cone, described by the radius of extension of the disease (between 0.5 and 1.5 mm), in which the tissue was modeled with weaker properties to represent the pathologic tissue (Table 1).

Generic implants with an elliptical cross-section were used instead of commercial rings to focus on studying size and diameter of the implants. Still, dimensions and volumes of the generic implants were similar to those of their analogous commercial rings (Fig. 1e and Supplementary Tables S1–S3). Three different typologies were considered: generic intrastromal continuous rings implanted in a pocket (gICRP; analogue to MyoRing), generic intrastromal continuous ring implanted in a tunnel (gICRT; analogue to a 355° Keraring), and 2 symmetric 150° generic intrastromal ring segments (gIRS; analogue to Intacs/Ferrara inserts). Pocketing procedure was assumed to be performed with a femtosecond laser generating stromal bubbles with a size between 1 and 5 µm.[27] The diameter of the intrastromal pocket (Φ_{Pocket}) was set to 8 mm and its thickness (T_{Pocket}) to 5 µm[4]. The diameter of the intrastromal tunnel (Φ_{Tunnel}) varies to match the implanted segment. For all configurations, the implantation depth varied between 55% and 75% of the stromal thickness (see Table 2 for more details on the simulated scenarios).

In silico models were built in Abaqus (Dassault Systèmes, France) using the finite element (FE) method. This modeling approach allows the calculation of the complex mechanical interaction between the corneal tissue and the implants placed in the stromal bed. Taking advantage of the symmetry for the different ring typologies (Fig. 1a.2), the in silico model of the cornea can be reduced to a symmetric model, saving computational resources and time. For IRS, the cornea was reduced to a three-dimensional symmetric quarter model by applying appropriate symmetry boundary conditions. For continuous rings, the symmetry of revolution around the visual axis was exploited to simulate the full corneal response by using a simple two-dimensional section (Fig. 1a.2). A physiological IOP of 15 mm Hg was set as loading condition in the posterior surface of the cornea. Corneal tissue was prestretched to its nominal IOP by using an iterative algorithm.[28,29] After pressurization of the cornea, the elements of the pocket (respectively tunnel) were removed, the stroma separated using a simulated surgical tool, and the implants lodged in the corneal stroma either in a pocket or a tunnel (Figs. 1b–1d, and Supplementary Fig. S1).

The stroma of the cornea with high myopia was considered as a normal tissue, whereas KC presented a central area (Φ_{KC}) with degenerated mechanical properties. Although cornea is highly anisotropic owing to the collagen fiber distribution,[30,31] it is not possible to introduce the distribution of corneal collagen fibers in an axisymmetric model. A Yeoh isotropic hyperelastic strain energy function[32] was used to simulate the mechanical behavior of the corneal stroma. Further information regarding the in silico model (mesh, material model, or boundary conditions) can be found in the Supplementary Figure S1.

Optical and Mechanical Analysis

The analysis of the results of the in silico models was done using the following optical parameters: the average curvature of the central cornea (K_{mean}) and the SE. K_{mean} was calculated using the concept of simulated keratometry[33] in which only the refraction of the central part of the anterior cornea is used:

$$K_{mean}(D) = \frac{n-1}{R}$$

where n = 1.3375 is the keratometric index of the cornea, R is the radius of curvature (in meters) of the

Table 2. Summary of the Parameters Used for the Simulation of Each Scenario

#	Z [%]	Φ_{Tunnel} [mm]	H [µm]	α_M [°]	Cornea	Surgery	Ring	Goal
1	55, 60, 75	6	200	25.9	Myopia	Pocket Tunnel	Continuous Segment	Implantation depth
2	75	5, 6, 7	200	25.9	Myopia	Pocket Tunnel	Continuous Segment	Ring diameter
3	75	6	150, 200, 300	25.9	Myopia	Pocket Tunnel	Continuous Segment	Ring size
4	75	6	200	0, 12.5, 25.9, 37.5	Myopia	Tunnel	Segment	Postsurgical rotation of the ring in the stroma
5	75	6	200	25.9	Myopia	Pocket	Continuous	Circadian variation of IOP[41]
6	75	6	300	25.9	Myopia KC	Pocket Tunnel	Continuous	Corneal strengthening (SFC_{3D})
7	75	5, 6	200	25.9	Myopia KC	Pocket Tunnel	Continuous	Normal vs. pathologic corneas

The geometric parameters are described in Figure 1. Additional information can be found in the Supplementary Material (Supplementary Tables S1–S3).

sphere that best fits of the anterior corneal surface in a diameter of 3 mm around its center.

The wavefront error of the optical system was calculated using an in-house ray tracing algorithm[34] and fitted using Zernike polynomials[35] to calculate the SE,[36]

$$SE\,(D) = \frac{-4\sqrt{3}\cdot Z_2^0}{r_0^2}$$

where Z_2^0 (µm) is the Zernike coefficient corresponding to the defocus and r_0(mm) is the radius of the exit pupil of the optical system.

The mechanical analysis of the cornea was inspired by the concept of corneal strengthening factor (SFC) introduced by Daxer.[18] In this study, a generalized three-dimensional distribution of the local strengthening factor (SFC_{3D}) was used rather than a single value describing the global behavior of the implant, which allows us to quantify the mechanical effect of ring implantation. In short, the SFC_{3D} was defined as the ratio of an equivalent stress at the centroid of each FE, after (σ_{SFC}^{post}) and before (σ_{SFC}^{pre}) the insertion of the implants:

$$\sigma_{SFC} = \sqrt{(\sigma_1 - \sigma_2)^2 + (\sigma_1 - \sigma_3)^2 + (\sigma_2 - \sigma_3)^2}$$

$$SFC_{3D} = \frac{\sigma_{SFC}^{post}}{\sigma_{SFC}^{pre}}$$

where σ_i are the maximum principal stresses in directions (i = 1,2,3). Therefore SFC_{3D} >1 implies an increased stress in the stroma after implantation, whereas SFC_{3D} <1 corresponds to a relaxation of the corneal stroma.

The probability of corneal stiffening —$p(SFC_{3D} \geq \Theta)$— was derived from SFC_{3D} as a quantification of the overall increase of corneal stresses. $p(SFC_{3D} \geq \Theta)$ measures the volume of corneal tissue that presents a postsurgical strengthening factor above a given threshold Θ. For example, $p(SFC_{3D} \geq 2)$ reports the volume of corneal tissue with a postsurgical stress two times higher than in the presurgical configuration.

Model Calibration and Validation

MyoRing simulations were performed to calibrate the numerical model against clinical data, and to provide a numerical benchmark to compare generic implants. Tissue properties of the numerical model were calibrated using clinical data available for two eyes of the same patient treated for high myopia using a MyoRing of 280-µm thick and 5 mm in diameter, which were implanted inside an 8-mm intrastromal pocket.[4] The average changes in the central curvature, δK_{mean}, were 4.9 and 4.8 D for the right and left eye, respectively. Presurgical in silico models were built for both eyes and the mechanical properties of the corneal stroma were adjusted using an iterative optimization procedure until the postsurgical in silico outcomes matched the clinical data.[34] Optimal mechanical properties were determined when, for both eyes, the K_{mean} obtained numerically matched the clinical measurement with a precision below the resolution of clinical topographers (±0.25 D).

After calibration of the mechanical behavior on these two eyes, the behavior of the in silico model was verified using retrospective data obtained on 15 patients treated with MyoRing for high myopia.[10] A virtual cohort of patients with high myopia (SE: 10 ± 2 D) was created using the following population data: central corneal thickness (CCT) (525 ± 31 µm),[37] K_{mean} (44.5 ± 1.5 D), axial length (26 ± 1 mm),[37] and anterior chamber depth (3.3 ± 0.42 mm).[38] Each virtual patient received a 280-µm MyoRing with a diameter of 5 mm, and the change in SE (δSE) was used to compare the predictions of the numerical model with the published clinical data.

Mechanical properties for the pathological tissue were calibrated using a similar optimization procedure to the one introduced by Kling and Marcos[9] in which the normal mechanical properties were reduced by a factor F of up to 100. Starting from a normal in silico model (K_{mean}: 45 D), a tissue weakening was introduced in the region Φ_{KC} of the predefined KC. The mechanical properties of the weakening were iteratively modified until the K_{mean} for the KC reached a typical value of 50 D.[39,40] The material properties for the cone were accepted once the calibration error was below ±0.25 D.

In Silico Scenarios

Seven scenarios were designed to assess the effects of (1) ring design and positioning (scenarios #1–#4 in Table 2), and (2) the biomechanical environment (scenarios #5–#7 in Table 2). First, the geometric parameters of the intrastromal rings and the surgical procedure were studied, such as the individual effect of the implantation depth (scenario #1), diameter of the ring (scenario #2), and the size of its cross-section (scenario #3). Also, the rotation of the ring after surgery was studied for different manufacturing angles of the cross-section (scenario #4). These evaluations were performed on a cornea having a high myopia. Continuous rings inserted in a tunnel and in a pocket, as well as ring segments inserted in a tunnel were

Table 3. Material Parameters for Normal and Pathological Tissue

Topology	Tissue	E_P [kPa]	C_{10} [kPa]	C_{20} [kPa]	C_{30} [kPa]
High myopia	Normal	214 (100%)	35.5	3.2	1.9
$KC_{0.5}$	Severe weakness	14 (7%)	2.1	0.2	0.1
KC_1	Mild weakness	65 (30%)	10.7	1.0	0.6
$KC_{1.5}$	Low weakness	118 (55%)	19.5	1.8	1.0

KC presents different degree of tissue weakening depending on the affected area of the cornea (Φ_{KC}). E_P: tangent modulus at the physiological prestretch; C_{10}, C_{20}, C_{30}: parameters of Yeoh material model. Compressibility of the cornea, D_k, was set to 10^{-5} (MPa^{-1}) to model a nearly incompressible tissue.

studied. The second set of scenarios focused on the effect of the biomechanical environment on the surgical outcomes. Specifically, we studied the effect of the circadian variation of IOP (scenario #5), the stress increase after ring implantation (scenario #6), and the impact of tissue mechanical properties (scenario #7) on the optical and mechanical outcomes of the procedure. In particular, the scenario #7 compared the effect of the treatment between normal mechanical properties found in myopic cases with pathologic properties found in KC corneas.

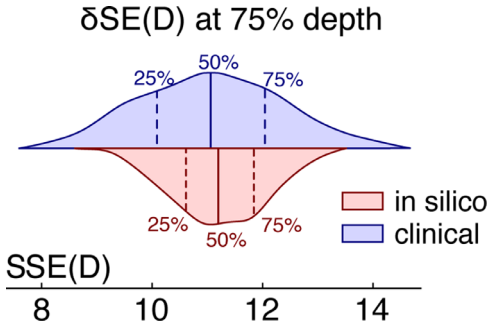

Figure 2. Validation of in silico model. In silico models (*red*) predict the change in SE (δSE) observed clinically (*blue*).[10]

Results

In Silico Model Validation

The properties describing the mechanical behavior of normal corneas sustaining MyoRing implantation were identified on two eyes. The iterative approach used to identify the mechanical properties describing the pathologic was able to reproduce the morphologic alteration observed in KC patients. The K_{mean} obtained at the end of the identification was 50 D, and the identified properties resulted in an important reduction of the stiffness of the tissue[9,42] (Table 3). The tangent modulus at the corneal prestretch (E_P) was used to provide an estimate and compare the biomechanical response of the tissue in the different cases.[43]

The assessment of the predicting power of this model conducted on a cohort of patients with high myopia showed that the numerical model was able to predict the change in SE measured on patients treated with MyoRing,[10] with an overall prediction error below 0.6 D (Fig. 2).

Ring Design and Position

Depending on the selected surgical technique, the change in surgical spherical equivalent (δSE) was driven by a different set of factors. For implants in intrastromal tunnel (gIRS, gICRT), the size and diameter of the implant were the most important factors affecting δSE, whereas the intrastromal implantation depth did not affect when implanted following clinical recommendations (blue and orange lines in Figs. 3a, 3c). The amount of correction ranged between 1 and 3.5 D (Figs. 3b, 3c) when individually increasing the size or decreasing the diameter of the implant. For implants inserted in intrastromal pocket (gICRP), all the parameters contributed to the change in refraction. A 20% variation in depth would have a noticeable impact on visual acuity of up to 5 D (Fig. 3a). δSE decreased for larger ring diameters with a change of up to −4 D when the diameter of the implant increased from 5 to 7 mm (Fig. 3b). δSE increased for bigger diameters with a change up to +6 D (Fig. 3c).

Once the influence of the intrastromal depth is ruled out by selecting the surgical technique, the size and diameter of the implant remain as the most important parameters controlling the refraction. For a given implantation depth of 75% of the stromal thickness, Figure 4 represents a generic nomogram in which δSE can be determined based on the surgical procedure and different combinations of implant size and diameter. There are regions in which the δSE can be kept constant by nonlinearly increasing (resp. decreasing) the size of the cross-section, whereas increasing (resp. decreasing) the diameter or, i.e., the distance from the local effect of the ring to the corneal center where the

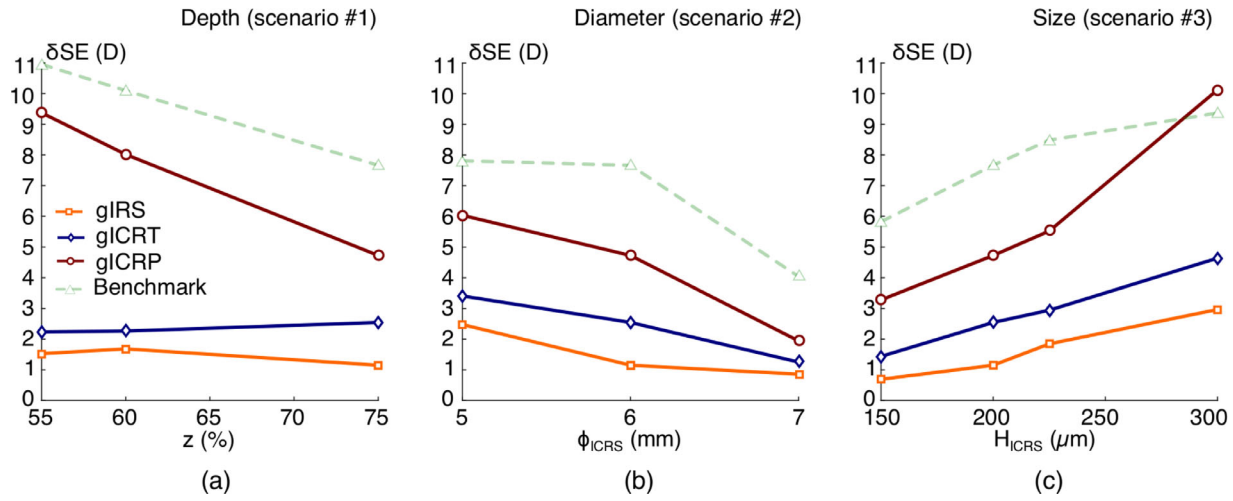

Figure 3. Main individual effect of design and positioning on the change in SE (δSE) between pre- and postsurgical corneas (scenarios #1–#3). (**a**) Influence of intrastromal depth of implantation on δSE; (**b**) influence of the diameter of the implant on δSE; (**c**) influence of the size of the implant on δSE. Results are reported for gIRS (in *orange*) and generic continuous ring in tunnel (gICRT in *red*), and in a pocket (gICRP in *blue*). Results for the MyoRing (*dashed green*) are reported for comparison purposes.

refraction occurs. Care must be taken as this nonlinear correlation includes factors such as the IOP or the mechanical properties of the stroma. Although trends were similar for all the typologies, implants in tunnel were able to achieve only up to half of the correction achieved with continuous rings in pocket. In our case, this higher refractive correction can only be associated to the mechanical effect of the intrastromal pocket.

The postsurgical rotation of the ring (α_S) was mainly determined by the manufacturing angle (α_M) of the ring's cross-section (Fig. 5). The highest postsurgical rotation was close to 20° when the ring was designed without consideration for the corneal curvature ($\alpha_M = 0°$). Cross-sections with a manufacturing angle that was tangential to the curvature of the posterior corneal surface ($\alpha_M \sim 25°$) presented a postsurgical rotation close to zero. These results indicate that a threshold at approximately 25° determines whether the ring would rotate toward the corneal center ($\alpha_M < 25°$) or toward the periphery ($\alpha_M > 25°$). Postsurgical intrastromal rotation of the implant could induce between 1 and 2 D of uncontrolled refractive correction.

Effect of Corneal Biomechanics

A circadian variation of IOP of ±20% around the baseline of 15 mm Hg[41] induced a physiological radial displacement in the surroundings of the implant for the presurgical cornea whose vertical component (i.e., vertical displacement) was approximately 40 μm. Right after laser pocketing, the cornea was mechanically weaker due to tissue vaporization and experienced a 50% increase in vertical displacement (~60 μm) at the same location, which decreased to a 25% (~50 μm) after continuous ring implantation regardless of whether it was implanted in pocket or tunnel (gICRP and gICRT). The vertical displacement of continuous rings occurred simultaneously with a radial expansion of the cornea under the variation of IOP. As continuous implants are much stiffer than the cornea and can only displace in vertical direction, gICRP experienced a tangential sliding of 30 μm inside the pocket due to this corneal radial expansion (not present for gICRT implanted in tunnel).

Circadian corneal kinematics further impacted visual perception. Attending to the amount of refractive error induced by 1 mm Hg increment (δSE/δIOP), normal corneas presented refractive stability against IOP variations (0.03 D/mm Hg). Because of the corneal weakening derived from the pocketing procedure, this ratio increased up to 0.2 D/mm Hg. Right after ring implantation, ratios increased up to 0.67 D/mm Hg for gICRT and up to 0.83 D/mm Hg for gICRP. Daily variations of IOP induced a similar displacement in the region of the implantation, either there was implant or not, but the refractive error was greatly affected in corneas with implants.

Mechanically, corneas did not present a dramatic increment on stromal stresses at the corneal center after ring implantation, but just a slight relaxation in a small volume of tissue for gICRP implantations (SFC ~0.9). The three-dimensional distribution of the corneal strengthening factor (SFC_{3D}) outlined that the main stiffening effect occurred in the surroundings of the implant, whereas the center of the cornea did

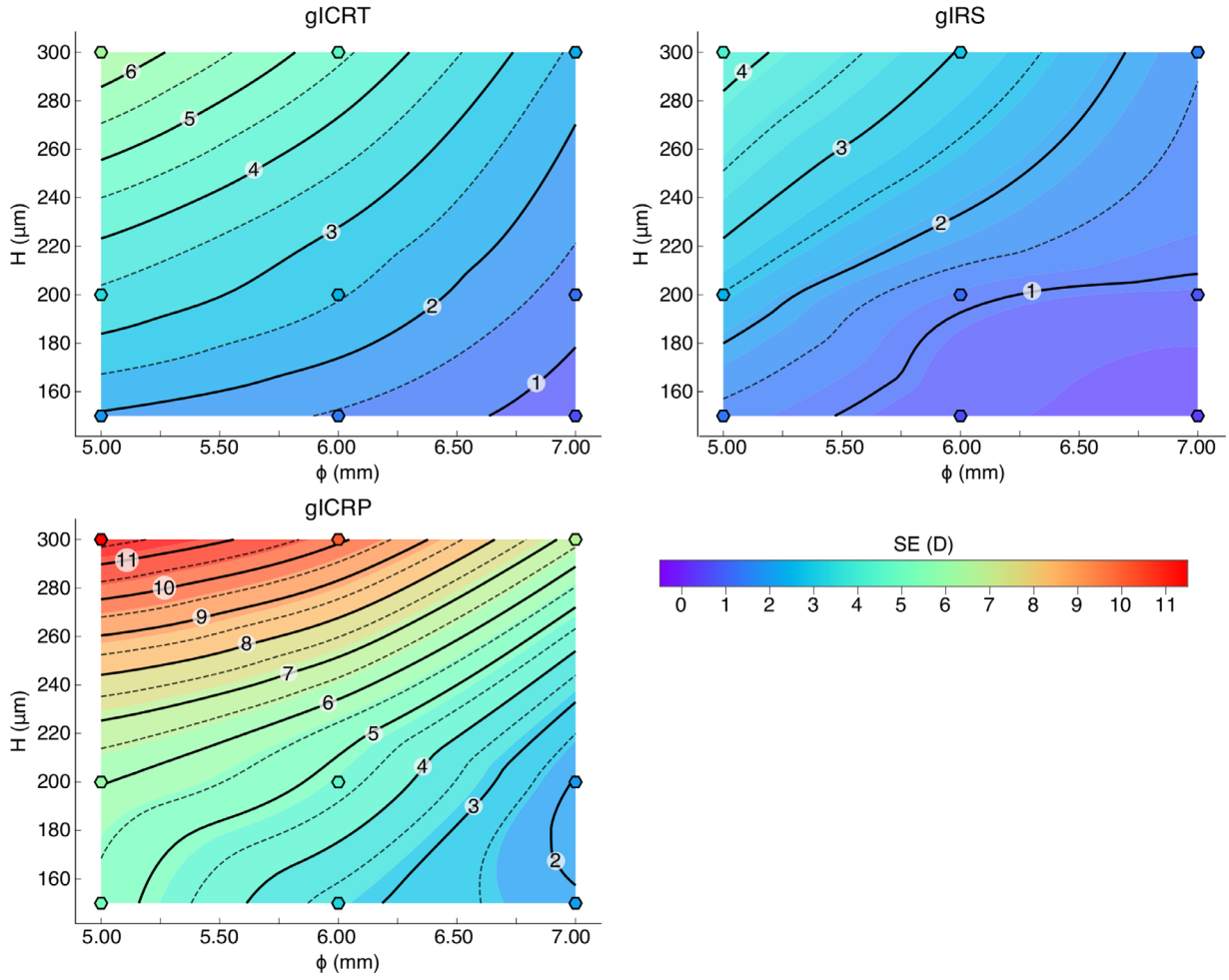

Figure 4. Effect of the interaction between size and diameter of the implant on the change in SE (δSE) between pre- and postsurgical corneas (scenarios #2–#3). Simulations combined different ring sizes (150, 200, and 350 µm) and diameters (5, 6, and 7 mm) for a given intrastromal depth of 75% of the stromal thickness. gICRT: generic intrastromal continuous tunnel; gICRP: generic intrastromal continuous ring in pocket; gIRS: generic intrastromal ring segment. *Dashed contour lines* represent increments of +0.5 D.

not present a strengthening greater than 1.5 (Fig. 6). Moreover, the likelihood of finding corneal strengthening factors greater than 2 at the central cornea was almost nonexistent for all typologies (gICRT and gICRP in Fig. 6; gIRS in Supplementary Fig. S2). Accounting for the diminished mechanical properties in KC did not affect the SFC_{3D}, nor the probability of finding strengthening values higher than 2. Corneal strengthening values for the rest of the combinations are provided as Supplementary material (Supplementary Table S4).

The intrastromal pocket introduced a discontinuity in the Cauchy stress distribution of the cornea that resulted in higher stresses in the posterior stroma, whereas the anterior stroma slightly relaxed (max. ~10% relaxation). Such discontinuity was even more noticeable when the pathological weakening of a KC was present (Fig. 6). When a gICRT was implanted, the SFC_{3D} gradient at the corneal center was smooth and mostly homogeneous through the corneal cross-section even if a biomechanical discontinuity such a central KC was present. In any case, the SFC_{3D} at the center never exceeded 1.5, even for the most severe cone (Supplementary Table S4), which indicates that the pre- and postsurgical stress distribution was only slightly affected by the ring implantation at the corneal center.

Trends for the correction of the SE (δSE) were not sensitive to the change in biomechanical properties of the tissue or the extension of the disease, and therefore the refractive correction for each simulated patient was similar (Fig. 7). Changing the ring design and position introduced similar refractive changes for normal and pathological corneas. As outlined previously (Fig. 3), changing the diameter of the implant from 5 to 6 mm introduced a constant shift in δSE (~2 D for gICRP; ~3 D for gICRT). A change

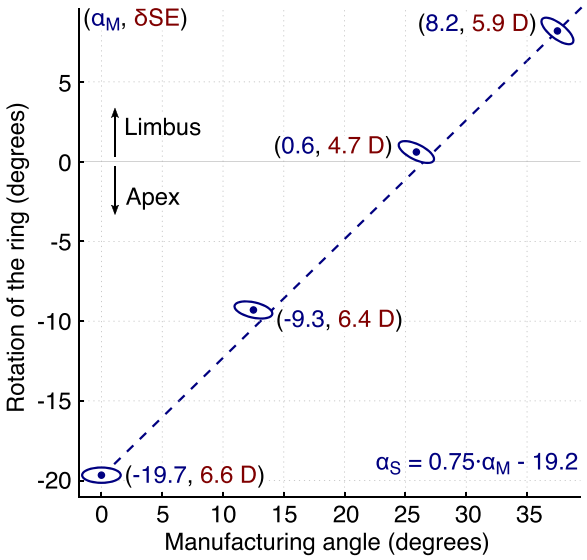

Figure 5. Postsurgical rotation (α_S) of gIRS depending on the manufacturing angle (α_M) of the cross-section (scenario #4). Cross-sections were oriented according to manufacturing angles of 0°, 12.5°, 25.9°, and 37.5°. Positive rotations turn gIRS toward the limbus, whereas negative rotations turn gIRS toward the corneal center.

in the shape of the cross-section from elliptical to MyoRing introduced a constant shift of approximately 0.75 D.

For both high myopia and KC, continuous rings introduced a fairly constant δSE between 10 and 11.5 D, which corrected the presurgical SE with a maximum error of 0.6 D for high myopia (SE, −9.4 D) and of 0.8 D for KC (SE, −11.9 D for $KC_{1.0}$). However, ring implantation in tunnel fell short of the targeted SE by 50% (5-mm diameter) and 100% (6-mm diameter), presenting a refractive correction that was mostly constant across changes in mechanical properties and extension of the disease.

Discussion

An in silico model of the cornea was used to study corneal mechanics after intrastromal ring implantation and to analyze the individual impact of the implant design and surgical parameters on the optical and biomechanical outcomes of the procedure, which is not directly possible in clinical practice. We hypothesized that implants do not strengthen the cornea globally but introduce a localized mechanical deformation that regularizes the corneal surface by adding volume to the stroma. The correction achieved by the implantation therefore depends on the amount of added volume and the distance from the corneal center at which they are implanted.

In silico simulations showed that the stress in the stroma was mostly modified in the surroundings of the implant with little to no impact on the level of mechanical stress in the central region of the cornea. This fact implies that the improvement of the optical outcomes does not result from an overall strengthening of the stromal tissue, but from localized mechanical deformations. The low dependence of the change in SE to variations of the mechanical properties of the stroma, even for the large reduction on the mechanical properties used to simulate the different KC cases, supported this finding.

In addition, considering that an implant only modifies the stress in the vicinity of its implantation, the change in the corneal shape does not result from a general stretching of the tissue but it is rather a consequence of the increased volume associated with it. Our results showed that the surface regularization induced by this bulkening effect is associated with a change of the optical properties, which is stronger when the ring is placed close to the corneal center and to the anterior surface, as well as for larger ring heights. Our hypothesis is also supported by clinical nomograms[4,5,7] in which the amount of correction is controlled by the appropriate selection of the ring thickness and diameter. In particular, simulations showed refraction changes of approximately 1.5 D per mm increase in diameter and 0.05 D per µm increase in thickness.

The main difference between surgical techniques is related to the presence of a pocket. Unlike intrastromal tunnels, cutting a pocket across the corneal stroma induces a discontinuity in the stress distribution, which limits the transmission of shear stresses across the cut interface and reduces the apparent corneal stiffness (Fig. 8). This reduced load-bearing capability makes the cornea more compliant, and therefore presenting less resistance to the bulkening effect induced by the implant, which allows to achieve higher refractive corrections. Although from a mechanical standpoint the corneal center is barely affected by the treatment, if we assume that KC growth is triggered by an increased level of stress in the tissue and that it develops anteriorly, our results suggest that only intrastromal pocketing could have the potential of limiting KC progression as stress would relax in the anterior stroma.

The presence of the intrastromal implants also modified the physiological kinematical response of the cornea. Our results showed that although a normal cornea would not present a noticeable change in refraction due to circadian variations in IOP (0.03 D/mm Hg), corneas with an implant would present a modified kinematics that would introduce a great change in refraction (0.8 D/mm Hg). This behavior is a direct consequence of the rigidity of the implant that restricts

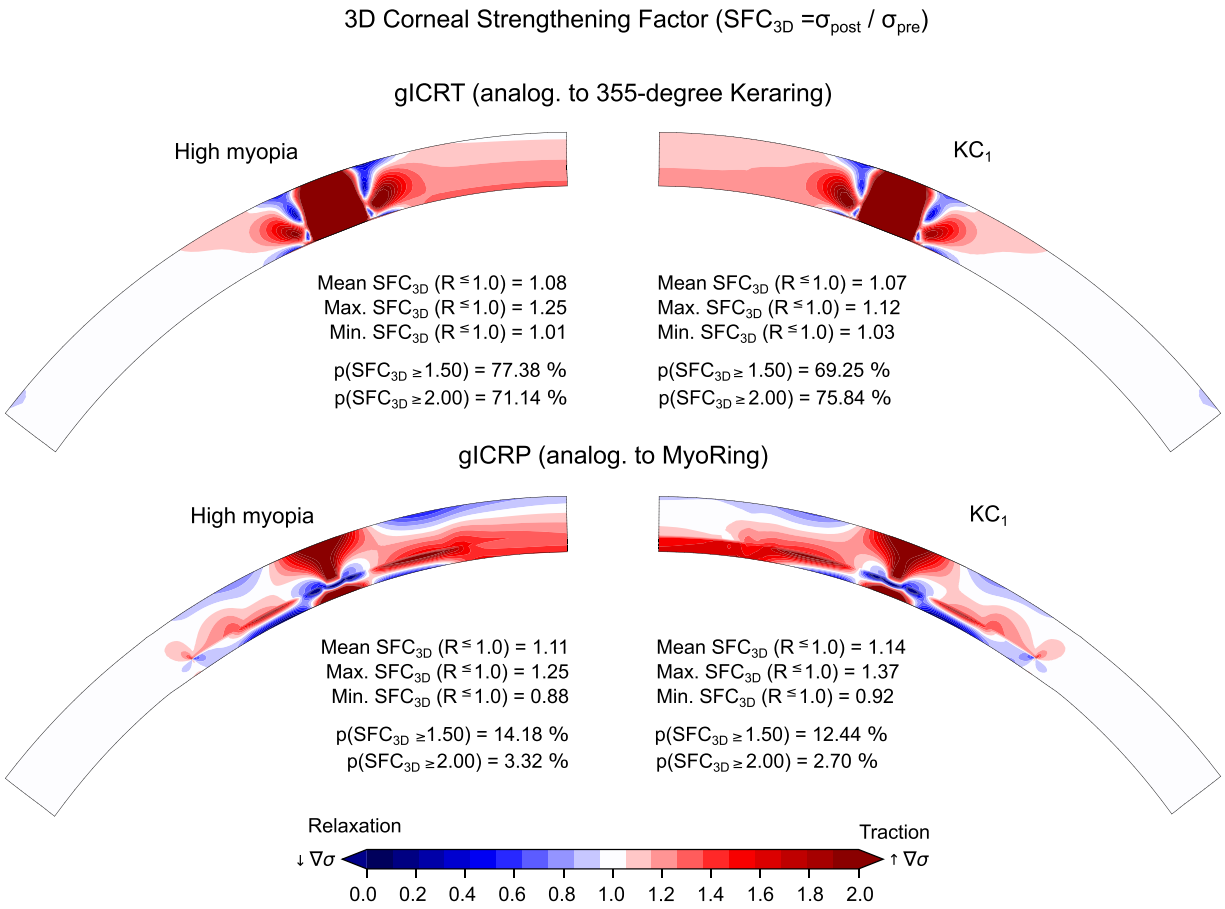

Figure 6. Spatial distribution of corneal strengthening factor (SFC_{3D}). SFC_{3D} after implantation of generic intrastromal continuous ring in tunnel (gICRT, *top*) and a generic intrastromal continuous ring in pocket (gICRP, *bottom*). The overall mechanical strengthening is similar for the high myopic cases (*left*) and for the pathological cases that have weakened mechanical properties in the central cornea (*right*).

the physiological radial and circumferential displacements (Fig. 8). In the surroundings of continuous implants, and because their diameter remains constant, changes in IOP will no longer deform the cornea in radial direction but in vertical direction. For implants in intrastromal pockets, a possible stromal sliding might occur depending on the friction between the ring and the stroma. Thus the overall spherical shape of the cornea cannot be preserved resulting in a straightening of the peripheral region of the tissue and a flattening of its central part. In this context, the implant acts as a dynamic pivot that can move and rotate within the corneal stroma modifying corneal kinematics. However, it is important to note that the ring cannot be considered as an auxiliary limbus because it moves during circadian variation of the pressure, even if this motion is restricted along the visual axis.

At a population level, our calibrated in silico model was able to predict the refractive correction in high-myopic patients with MyoRing. Also, optical results for generic rings were in good agreement with different clinical studies in which little difference between healthy and keratoconic outcomes at a population level was reported.[5,8,10,17,44,45] Unfortunately, clinical studies often report mixed ring typologies, corneal geometries, and degrees of pathology, and therefore results for keratoconic corneas would require of an in silico population study to fully support this conclusion.

The size of the cross-section and the diameter of the implant regulated the amount of refractive correction as reported by many authors. Recommended intrastromal implantation depths are close to the posterior corneal surface (~70%), which creates an uneven distribution of tissue above and below the implant that stabilizes it. For ring segments implanted within an optimal clinical range (60%–79%), refractive correction did not vary with implantation depth as reported by Hashemi et al.[11] For continuous implants in pocket, our results suggest that the refractive correction could increase up to approximately 100% if implants were to be placed at shallower depths (~50%) instead of at deeper depths, which could be one of the reasons why

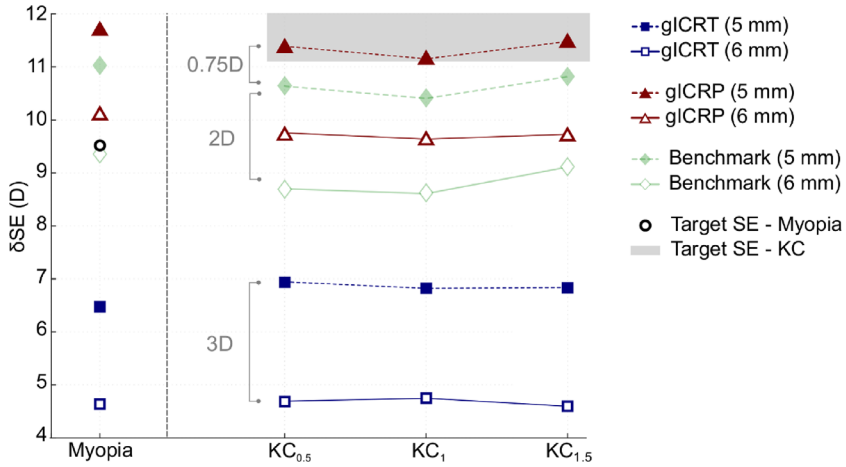

Figure 7. Impact of the stromal biomechanical properties on refractive outcomes after continuous ring implantation (diameter of the implant of 5 and 6 mm, 75% depth, and 300 µm size). The change in SE (δSE) was calculated for different severity of KC ($KC_{0.5}$, KC_1, and $KC_{1.5}$), as well as a reference cornea with high-myopia. Results for the MyoRing (*dashed green*) are reported for comparison purposes.

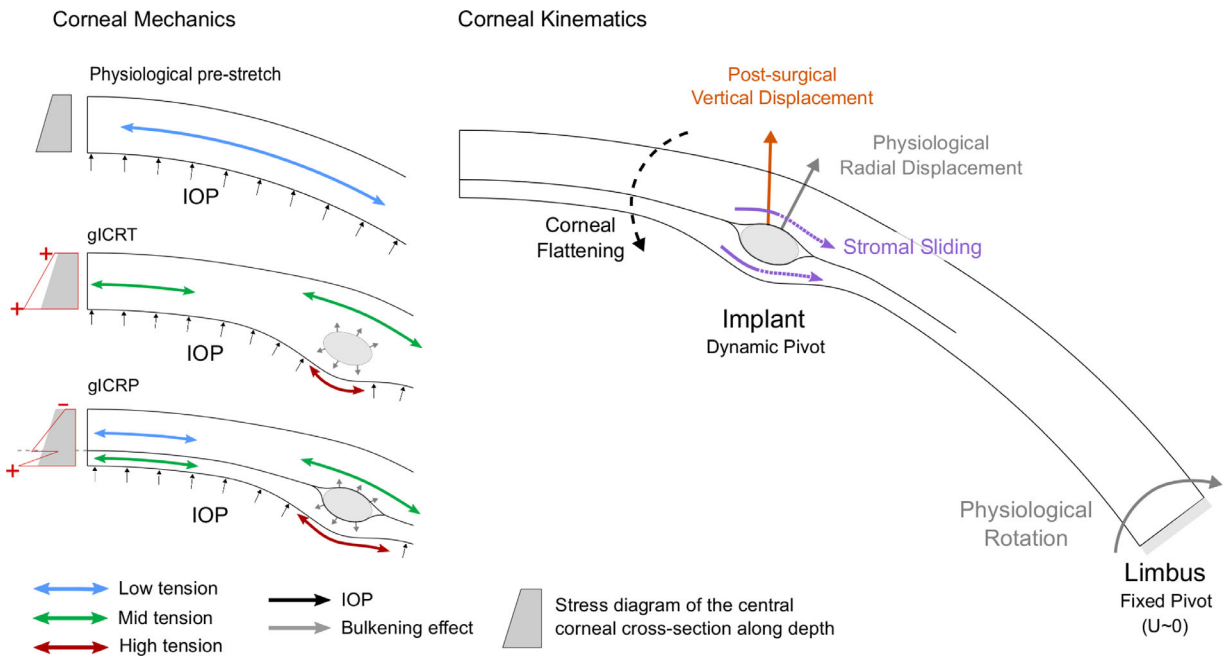

Figure 8. Diagram of corneal kinematics and mechanics after ring implantation (based on FE simulations). (Corneal mechanics, *left*) Physiological prestretch of the cornea due to IOP induces a membrane stress with a homogeneous distribution of stromal stress. gICRT increased the corneal stress and slightly thinned the cornea. gICRP increased the stress in the posterior stroma but relaxed it in the anterior stroma, and slightly thinned the cornea. Bulkening effect (pushing the corneal stroma, *gray*) created an uneven stress distribution above and below the implant. Stromal pocket introduced a shear stress discontinuity at the interface. (Corneal kinematics, *right*) Limbus acts as a fixed pivot point (no displacement) around which the cornea can adapt to balance mechanical changes. An intrastromal implant introduces a dynamic pivot (it can move and may rotate) that changes the physiological corneal kinematics by modifying how the stroma can adapt and move in its surroundings. As a result, cornea flattens. However, this effect is local and loses strength when the implant is located far from the corneal center.

MyoRing is advised to be placed at 300 µm with respect to the anterior surface.[18] Postsurgical rotation of ring segments in the stroma was driven by the manufacturing angle of the cross-section (α_M). Implants that were tangent to the curvature of the posterior corneal surface (α_M ~26°) presented higher stability. Because of the local stress distribution, the overstressed corneal stroma results in forces and angular momentum on the implant, which will tend to rotate inside the cornea, as reported by Ibares-Frías et al.[13]

Mechanically, our results showed that implants did not result in a remarkable change of stresses at the corneal center, which is not in agreement with current literature. Daxer[18] suggested that continuous rings should act as an auxiliary limbus that constraints and strengthens the cornea by limiting its movement. However, his initial approach used the Laplace equation, which disregarded complex physics (e.g., the interaction between the implant and the stroma, or the stress distribution in corneal thickness) and characterized the mechanical behavior of the whole cornea as a single ratio between the diameter of the cornea and the diameter of the implant. Our results showed that the level of stress at the corneal center remains close to presurgical values with strengthening values of less than 1.5, and that the ring could move along with the corneal stroma even if it modifies corneal kinematics.

To the best of our knowledge, few in silico studies introduced actual solid implants on the stroma and they only addressed continuous rings using axisymmetric simulations.[9,24,26] All mechanical models were isotropic hyperelastic and, some of them, neglected the corneal prestretch owing to the IOP.[9,24] Kahn and Shiakolas,[24] Ebrahimian et al.,[26] and Kling and Marcos[9] came to the conclusion that for the smallest diameters, implants could change refraction approximately 10 D for KC and 12 D for normal corneas, whereas for the largest optical zones implants were not effective (0.5 D). All these numerical results are in good agreement with the results provided in the present study.

Although our in silico model was able to reproduce the clinical data described in a small cohort study, it is not exempt of limitations. The main limitation is that the geometry of the model is based on an idealized spherical representation of the cornea that prevents evaluating changes in astigmatism after ring implantation. Other limitations are related to the mechanical material model used for describing the mechanical response of the cornea. First, unless used with care, axisymmetric models could provide a stiffer mechanical response than three-dimensional models. Second, to use axisymmetric models and alleviate the computational costs, we did not use a fiber-reinforced anisotropic model that accounted for the collagen network within the cornea. Although this assumption might modify postsurgical mechanical outcomes in the surroundings of the surgery and might fine-tune optical outcomes (mostly related to astigmatism), we do not expect a change in the global trends as we are comparing pre- and postsurgical situations at the central cornea in which the stress state is not greatly modified. Third, the mechanical model for KC was not validated but just calibrated to reproduce the typical curvature reported for KC patients. A proper morphological and mechanical characterization of the cone is needed to assess these particular patients. Nevertheless, the range of variation of mechanical stiffness for the cone ranged from 10% to 50% of the normal corneal stiffness,[9,42] which should encompass the most extreme cases and ensure that our general conclusions hold.

Conclusions

This study showed that implants do not stiffen the cornea but rather create a local bulkening effect that regularizes the corneal shape, with a stronger effect when they are placed close to the central cornea and when their size is thicker. Implantation intrastromal depth does not play an important role for rings in tunnels when placed within the clinical range, whereas for implants in intrastromal pocket, shallower implantation depths could provide a higher refractive correction. The manufacturing angle of the cross-section could be the responsible of causing unexpected postsurgical rotations within the corneal stroma. Implants in intrastromal pockets yield the highest refractive correction and it could be the only surgical technique that might limit KC progression providing that it is stress-driven. Implants modify corneal kinematics but without restricting corneal motion: they only drive how corneal stroma can move and rotate in the surroundings of the implant, which in turn results in a corneal flattening and a surface regularization. In silico models are powerful tools to better understand corneal biomechanics and could be used to better plan patient-specific interventions, to create nomograms that explicitly account for mechanics, or to help to optimize the design of implants without need of expensive experiments.

Acknowledgments

The authors thank Albert Daxer for providing the MyoRing geometry, and David Pablo Piñero Llorens for the fruitful discussion.

Calculations were performed on UBELIX (http://www.id.unibe.ch/hpc), the high-performance computing cluster at the University of Bern. Part of the work was performed by the ICTS "NANBIOSIS" specifically by the High-Performance Computing Unit (U27) of the CIBER in Bioengineering, Biomaterials, and

Nanomedicine (CIBER-BBN) at the University of Zaragoza, Project DPI2017-84047-R.

Supported by the European Commission (H2020-MSCA-IF-2017, proposal 786692; MÁA-G); the Spanish Ministry of Economy and Competitiveness (BES-2015-073630; JF-L) and Project DPI2017-84047-R; Department of Industry and Innovation (Government of Aragón); and European Social Fund 2014-2020 (T24_20R).

Disclosure: **M.Á. Ariza-Gracia,** None; **J. Flecha-Lescún,** None; **P. Büchler,** None; **B. Calvo,** None

[#] MAA-G and JF-L contributed equally.

References

1. Rabinowitz YS. Keratoconus. *Surv Ophthalmol*. 1998;42(4):297–319, http://dx.doi.org/10.1016/S0039-6257(97)00119-7.
2. Akaishi L, Tzelikis PF, Raber IM. Ferrara intracorneal ring implantation and cataract surgery for the correction of pellucid marginal corneal degeneration. *J Cataract Refract Surg*. 2004;30(11):2427–2430, http://dx.doi.org/10.1016/j.jcrs.2004.04.047.
3. Yildirim A, Cakir H, Kara N, Uslu H. Long-term outcomes of intrastromal corneal ring segment implantation for post-LASIK ectasia. *Cont Lens Anterior Eye*. 2014;37(6):469–472, doi:10.1016/j.clae.2014.07.010.
4. Rattan SA. Continuous intracorneal ring implantation for treatment of myopic astigmatism. *Int Med Case Rep J*. 2018;11:217–220, doi:10.2147/IMCRJ.S173167.
5. Jadidi K, Nejat F, Mosavi SA, et al. Full-ring intrastromal corneal implantation for correcting high myopia in patients with severe keratoconus. *Med Hypothesis Discov Innov Ophthalmol*. 2016;5(3):89–95.
6. Yousif MO, Said AMA. Comparative study of 3 intracorneal implant types to manage central keratoconus. *J Cataract Refract Surg*. 2018;44(3):295–305, doi:10.1016/j.jcrs.2017.12.020.
7. Alaaeldin O, Seleet M, Soliman A. Femtosecond laser intracorneal ring segment implantation based on a nomogram modification in type 1 and type 2 ectasia. *J Egypt Ophthalmol Soc*. 2015;108(1):1–5, doi:10.4103/2090-0686.160328.
8. Janani L, Tanha K, Najafi F, et al. Efficacy of complete rings (MyoRing) in treatment of keratoconus: a systematic review and meta-analysis. *Int Ophthalmol*. 2019;39(12):2929–2946, doi:10.1007/s10792-019-01121-9.
9. Kling S, Marcos S. Finite-element modeling of intrastromal ring segment implantation into a hyperelastic cornea. *Invest Ophthalmol Vis Sci*. 2013;54(1):881–889, doi:10.1167/iovs.12-10852.
10. Daxer A. MyoRing treatment of myopia. *J Optom*. 2017;10:194–198, doi:10.1016/j.optom.2016.06.003.
11. Hashemi H, Yazdani-Abyaneh A, Beheshtnejad A, Jabbarvand M, Kheirkhah A, Ghaffary SR. Efficacy of intacs intrastromal corneal ring segment relative to depth of insertion evaluated with anterior segment optical coherence tomography. *Middle East Afr J Ophthalmol*. 2013;20(3):234–238, doi:10.4103/0974-9233.114800.
12. Barbara R, Barbara A, Naftali M. Depth evaluation of intended vs actual intacs intrastromal ring segments using optical coherence tomography. *Eye*. 2016;30:102–110, doi:10.1038/eye.2015.202.
13. Ibares-Frías L, Gallego P, Cantalapiedra-Rodríguez R, et al. Tissue reaction after intrastromal corneal ring implantation in an experimental animal model. *Graefe's Arch Clin Exp Ophthalmol*. 2015;253(7):1071–1083, doi:10.1007/s00417-015-2959-5.
14. Daxer A. Corneal intrastromal implantation surgery for the treatment of moderate and high myopia. *J Cataract Refract Surg*. 2008;34:294–298, doi:10.1016/j.jcrs.2007.10.011.
15. Abdellah MM, Ammar HG. Femtosecond laser implantation of a 355-degree intrastromal corneal ring segment in keratoconus: a three-year follow-up. *J Ophthalmol*. 2019;2019(6783181):1–7, doi:10.1155/2019/6783181.
16. Rocha GA do N, Ferrara de Almeida Cunha P, Torquetti Costa L, Barbosa de Sousa L. Outcomes of a 320-degree intrastromal corneal ring segment implantation for keratoconus: results of a 6-month follow-up. *Eur J Ophthalmol*. 2020;30(1):139–146, doi:10.1177/1120672118818018.
17. Daxer A, Ettl A, Hörantner R. Long-term results of MyoRing treatment of keratoconus. *J Optom*. 2017;10(2):123–129, doi:10.1016/j.optom.2016.01.002.
18. Daxer A. Biomechanics of corneal ring implants. *Cornea*. 2015;34(11):1493–1498.
19. Alio JL, Piero DP, Daxer A. Clinical outcomes after complete ring implantation in corneal ectasia using the femtosecond technology: a pilot study. *Ophthalmology*. 2011;118(3):1282–1290, doi:10.1016/j.ophtha.2010.12.012.
20. Alio J, Barraquer R, Esperanza S, Murta J, Teus M, Vega-Estrada A. Intrastromal corneal

ring segments: how successful is the surgical treatment of keratoconus? *Middle East Afr J Ophthalmol*. 2014;21(1):3, doi:10.4103/0974-9233.124076.
21. Vega-Estrada A, Alio J. The use of intracorneal ring segments in keratoconus. *Eye Vis*. 2016;3(8):1–7.
22. Bikbova G, Kazakbaeva G, Bikbov M, Usubov E. Complete corneal ring (MyoRing) implantation versus MyoRing implantation combined with corneal collagen crosslinking for keratoconus: 3-year follow-up. *Int Ophthalmol*. 2018;38(3):1285–1293, doi:10.1007/s10792-017-0593-4.
23. Lago MA, Rupérez MJ, Monserrat C, et al. Patient-specific simulation of the intrastromal ring segment implantation in corneas with keratoconus. *J Mech Behav Biomed Mater*. 2015;51:260–268, https://doi.org/10.1016/j.jmbbm.2015.07.023.
24. Kahn SN, Shiakolas PS. To study the effects of intrastromal corneal gin geometry and surgical condictions on the postsurgical outcomes through finite element analysis. *J Mech Med Biol*. 2016;16(7):1–16, http://dx.doi.org/10.1142/S0219519416501013.
25. Flecha-Lescun J, Calvo B, Zurita J, MÁ Ariza-Gracia. Template-based methodology for the simulation of intracorneal segment ring implantation in human corneas. *Biomech Model Mechanobiol*. 2018;17:923–938. https://doi.org/10.1007/s10237-018-1013-z.
26. Ebrahimian A, Mosaddegh P, Bagheri NM, Pirhadi S. A simple numerical approach to mimic MyoRing surgery in keratoconus corneas based on optical coherence tomography. *Cronicon EC Ophthalmol*. 2019;10(5):345–356.
27. Lubatschowski H, Maatz G, Heisterkamp A, et al. Application of ultrashort laser pulses for intrastromal refractive surgery. *Graefe's Arch Clin Exp Ophthalmol*. 2000;238(1):33–39, doi:10.1007/s004170050006.
28. Elsheikh A, Whitford C, Hamarashid R, Kassem W, Joda A, Büchler P. Stress free configuration of the human eye. *Med Eng Phys*. 2013;35(2):211–216, doi:10.1016/j.medengphy.2012.09.006.
29. Ariza-Gracia MÁ, Zurita J, Piñero DP, Calvo B, Rodríguez-Matas JF. Automatized patient-specific methodology for numerical determination of biomechanical corneal response. *Ann Biomed Eng*. 2016;44(5):1753–1772, doi:10.1007/s10439-015-1426-0.
30. Winkler M, Shoa G, Xie Y, et al. Three-dimensional distribution of transverse collagen fibers in the anterior human corneal stroma. *Invest Ophthalmol Vis Sci*. 2013;54(12):7293–7301, doi:10.1167/iovs.13-13150.
31. Forrester JV, Dick AD, McMenamin PGRF, Pearlman E. Anatomy of the eye and orbit. Forrester JV. *The Eye: Basic Sciences in Practice. Elsevier Health Sciences*. 2015:14–20.
32. Yeoh OH. Some forms of the strain energy function for rubber. *Rubber Chem Technol*. 1993;66(5):754–771, doi:10.5254/1.3538343.
33. Savini G, Hoffer KJ, Lomoriello DS, Ducoli P. Simulated keratometry versus total corneal power by ray tracing: a comparison in prediction accuracy of intraocular lens power. *Cornea*. 2017;36(11):1368–1372, doi:10.1097/ICO.0000000000001343.
34. Ariza-Gracia MÁ, Ortillés Á, Cristóbal JÁ, Rodríguez Matas JF, Calvo B. A numerical-experimental protocol to characterize corneal tissue with an application to predict astigmatic keratotomy surgery. *J Mech Behav Biomed Mater*. 2017;74:304–314, doi:10.1016/j.jmbbm.2017.06.017.
35. Lakshminarayanan V, Fleck A. Zernike polynomials: a guide. *J Mod Opt*. 2011;58(7):545–561, doi:10.1080/09500340.2011.554896.
36. Jaskulski M, Martínez-Finkelshtein A, López-Gil N. New objective refraction metric based on sphere fitting to the wavefront. *J Ophthalmol*. 2017, doi:10.1155/2017/1909348
37. Sorkin N, Rosenblatt A, Smadja D, et al. Early refractive and clinical outcomes of high-myopic photorefractive keratectomy as an alternative to LASIK surgery in eyes with high preoperative percentage of tissue altered. *J Ophthalmol*. 2019;2019, doi:10.1155/2019/6513143.
38. Fernández-Vigo JI, Fernández-Vigo JÁ, Macarro-Merino A, Fernández-Pérez C, Martínez-de-la-Casa JM, García-Feijoó J. Determinants of anterior chamber depth in a large Caucasian population and agreement between intra-ocular lens Master and Pentacam measurements of this variable. *Acta Ophthalmol*. 2016;94(2):e150–e155, doi:10.1111/aos.12824.
39. Cueto LF-V, Lisa C, Poo-López A, Madrid-Costa D, Merayo-Lloves J, Alfonso JF. Intrastromal corneal ring segment implantation in 409 paracentral keratoconic eyes. *Cornea*. 2016;35(11):1421–1426.
40. Kubaloglu A, Cinar Y, Sari ES, Koytak A, Ozdemir B, Ozertürk Y. Comparison of 2 intrastromal corneal ring segment models in the management of keratoconus. *J*

Cataract Refract Surg. 2010;36(6):978–985, doi:10.1016/j.jcrs.2009.12.031.

41. Ariza-Gracia MA, Piñero DP, Rodriguez JF, Pérez-Cambrodí RJ, Calvo B. Interaction between diurnal variations of intraocular pressure, pachymetry, and corneal response to an air puff: preliminary evidence. *JCRS Online Case Reports*. 2014;3(1):12–15.
42. Andreassen TT, Hjorth Simonsen A, Oxlund H. Biomechanical properties of keratoconus and normal corneas. *Exp Eye Res*. 1980;31(4):435–441, doi:10.1016/S0014-4835(80)80027-3.
43. Ariza-Gracia MÁ, Redondo S, Piñero Llorens D, Calvo B, Rodriguez Matas JF. A predictive tool for determining patient-specific mechanical properties of human corneal tissue. *Comput Methods Appl Mech Eng*. 2017;317:226–247, doi:10.1016/j.cma.2016.12.013.
44. Nobari SM, Villena C, Jadidi K. Predictability, stability and safety of MyoRing implantation in keratoconic eyes during one year follow-up. *Iran J Ophthalmol*. 2014;26(3):136–143.
45. Mohebbi M, Hashemi H, Asgari S, Bigdeli S, Zamani KA. Visual outcomes after femtosecond-assisted intracorneal MyoRing implantation: 18 months of follow-up. *Graefe's Arch Clin Exp Ophthalmol*. 2016;254:917–922, doi:10.1007/s00417-015-3231-8.
46. Gökgöl C, Diehm N, Büchler P. Numerical modeling of nitinol stent oversizing in arteries with clinically relevant levels of peripheral arterial disease: the influence of plaque type on the outcomes of endovascular therapy. *Ann Biomed Eng*. 2017;45(6):1420–1433, doi:10.1007/s10439-017-1803-y.